

Article

Visualization of Antimicrobial-Induced Bacterial Membrane Disruption with a Bicolor AIEgen

Chengcheng Zhou ^{1,*} , Zeyu Ding ¹, Qiaoni Guo ¹ and Meijuan Jiang ^{2,*}

¹ School of Chemistry and Chemical Engineering, Yangzhou University, Yangzhou 225002, China; mz120200676@stu.yzu.edu.cn (Z.D.); mx120200423@yzu.edu.cn (Q.G.)

² Department of Chemistry, The Hong Kong University of Science and Technology, Clear Water Bay, Kowloon, Hong Kong, China

* Correspondence: zhoucc@yzu.edu.cn (C.Z.); mjiangae@connect.ust.hk (M.J.)

Abstract: Gram-negative bacteria are difficult to kill due to their complex cell envelope, including the outer membrane (OM) and cytoplasmic membrane (CM). To monitor the membranolytic action of antimicrobials on Gram-negative bacteria would facilitate the development of effective antimicrobials. In this paper, an aggregation-induced emission luminogen (AIEgen) with microenvironment-sensitive properties was employed to indicate the interaction of antimicrobials with the OM and CM of Gram-negative bacteria. The damaged extent of OM and CM caused by antimicrobials with the change of dosage and incubation time can be visually captured based on the variation of two emission colors of IQ-Cm responding to OM-defective (green) and CM-disruptive bacteria (orange). Meanwhile, the activity assessment of antimicrobials can be easily realized within 1–2 h based on the distinct response of IQ-Cm to live and dead *E. coli*, which is much faster than the agar plate culture. This probe may shed light on the understanding of the interaction between the membrane-active antimicrobials and cell envelope of Gram-negative bacteria and contribute to the future development of antimicrobials.



Citation: Zhou, C.; Ding, Z.; Guo, Q.; Jiang, M. Visualization of Antimicrobial-Induced Bacterial Membrane Disruption with a Bicolor AIEgen. *Chemosensors* **2022**, *10*, 284. <https://doi.org/10.3390/chemosensors10070284>

Academic Editors: Zheng Zhao and Zijie Qiu

Received: 16 June 2022

Accepted: 14 July 2022

Published: 16 July 2022

Publisher's Note: MDPI stays neutral with regard to jurisdictional claims in published maps and institutional affiliations.

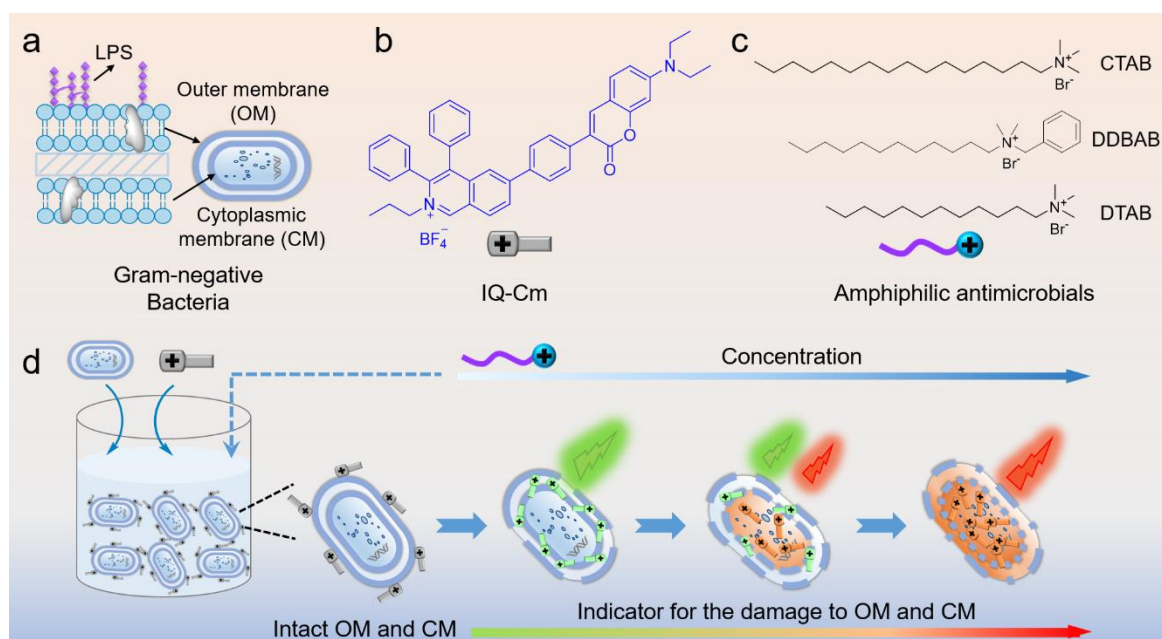


Copyright: © 2022 by the authors. Licensee MDPI, Basel, Switzerland. This article is an open access article distributed under the terms and conditions of the Creative Commons Attribution (CC BY) license (<https://creativecommons.org/licenses/by/4.0/>).

Keywords: membrane-active antimicrobial; aggregation-induced emission; Gram-negative bacteria; visualization; outer membrane; cytoplasm membrane

1. Introduction

Pathogenic microbes have greatly threatened human health and safety [1,2]. Especially, Gram-negative bacteria have caused a more critical healthcare issue, due to their complex cell envelope consisting of three essential layers: an outer membrane (OM), a cytoplasmic membrane (CM) and a peptidoglycan cell wall (Scheme 1a) [3]. Unlike CM, which is composed of the fluid phospholipid bilayer, OM possesses phospholipids in the inner leaflet and lipopolysaccharides (LPS) in the outer leaflet, which exerts the barrier function and makes Gram-negative bacteria difficult to kill [4,5]. Many Gram-negative bacteria have acquired resistance to the traditional antibiotics that act on specific intracellular targets [4,6,7]. To address this, membrane-active antimicrobials, such as the cationic amphiphiles, have been developed to physically disrupt bacterial membranes and thus show a low tendency to induce bacteria resistance [8–12]. When the antimicrobials compromise the CM integrity of Gram-negative bacteria, it is commonly regarded as the lethal event [4]. However, the existence of OM hinders the entry of antimicrobials to destroy the CM of bacteria, which often renders the designed antimicrobials invalid [5,13]. Thus, to facilitate the design and assessment of effective antimicrobials, it is necessary to monitor and understand the interaction of membrane-active antimicrobials with the OM and CM of Gram-negative bacteria.



Scheme 1. (a) Schematic cell envelope structure of Gram-negative bacteria. The molecular structures of (b) IQ-Cm and (c) chosen membrane-active antimicrobials. (d) Schematic illustration of IQ-Cm as an indicator of the membrane disruption of Gram-negative bacteria caused by membrane-active antimicrobials.

To monitor the bacterial membrane disruption of antimicrobials, some electrical devices [14,15], liquid crystals sensors [16] and fluorescence methods [17,18] have been explored. Fluorescence methods have attracted more attention not only due to the simple and fast feature, but also the direct visualization of the interaction between antimicrobials and bacteria [4,17,19,20]. Various fluorescent dyes, such as propidium iodide (PI), Rhodamine 123 and carbocyanine derivatives, have been developed to assess the viability and CM integrity of Gram-negative bacteria [18]. However, none of the above dyes can be solely used to offer information about the change of OM and CM simultaneously [21]. Two fluorochromes of OM and CM indicators must be adequately screened to avoid the wrong interpretations caused by the energy transfer phenomena between them [18]. Therefore, grasping the OM and CM variation based on one single fluorescence probe will greatly simplify the method and is highly desirable to better reveal the interaction of membrane-active antimicrobials with OM and CM of Gram-negative bacteria.

Aggregation-induced emission luminogens (AIEgens) have achieved great success in detecting microbes and bioanalytes due to their merits of low background and high sensitivity [22–27]. AIEgens with multi-rotor structures are normally non-fluorescent due to the fast dissipation of the excited state energy by the free intramolecular motions of their rotors, but become strongly emissive when the rotor motions are restricted by the surroundings [22,28]. Moreover, the multi-rotor structures make AIEgens highly sensitive to their surroundings [29,30]. When further bearing a twisted donor-acceptor structure, the AIEgens can respond to microenvironmental changes with different color emissions due to the twisted intramolecular charge transfer (TICT) effect [19,29,30]. These features make the AIEgens excellent candidates for visually monitoring the interaction of antimicrobials with Gram-negative bacterial OM and CM simultaneously. In this paper, a microenvironment-sensitive AIEgen, IQ-Cm, bearing a multi-rotor and twisted donor-acceptor structure, was employed to assess the antimicrobial-induced OM and CM disruption of Gram-negative bacteria by emitting two discernable colors, green and orange (Scheme 1). Chemically, IQ-Cm was composed of a cationic isoquinolinium moiety and a coumarin unit. IQ-Cm was demonstrated to rapidly assess the antimicrobial activity of the three chosen representative membrane-active quaternary ammonium antimicrobials (Scheme 1c). More

importantly, the damaged extent of OM and CM caused by antimicrobials can be visually grasped based on the diverse emission responses of IQ-Cm to the different physiological states of Gram-negative bacteria, i.e., normal, OM-defective and CM-disruptive ones (Scheme 1d).

2. Experimental Section

Materials: IQ-Cm was synthesized as reported previously [19]. Propidium iodide (PI) and three cationic antimicrobials, hexadecyl trimethyl ammonium bromide (CTAB), dodecyl dimethyl benzyl ammonium bromide (DDBAB) and dodecyl trimethyl ammonium bromide (DTAB), were purchased from Thermo Fisher and TCI, respectively, and used as received. The Gram-negative bacterium *E. coli* (JM109) was chosen as a representative. Phosphate-buffered saline (1× PBS, pH 7.4) was used throughout the work, unless otherwise noted.

Preparation of bacteria suspension: A single *E. coli* colony was added to 10 mL of Luria Broth (LB) culture, grown for 6–8 h under shaking (180–200 rpm) at 37 °C. *E. coli* was harvested by centrifugation at 7100 rpm for 2 min, washed once with PBS, and then re-dispersed in PBS. The optical density of the as-prepared *E. coli* suspension at 600 nm was adjusted to 1.0 ($OD_{600} = 1.0$) with PBS, which has about 10^8 CFU/mL of *E. coli*. For the preparation of the dead bacteria suspension, the harvested *E. coli* were treated with 200 µL of 75% alcohol solution for about 2–5 min, washed twice with PBS and re-suspended in PBS; it was kept on standby to determine the relationship of IQ-Cm emission intensity and dead bacteria number.

Evaluation of antimicrobial activity: The viability of *E. coli* treated with three cationic antimicrobials was assessed with IQ-Cm (or PI) probe and traditional agar plate culture. The effect of IQ-Cm itself on the viability of *E. coli* was evaluated by the traditional agar plate culture. **IQ-Cm (or PI) probe method:** *E. coli* suspensions ($\sim 2 \times 10^7$ CFU/mL) were treated with different concentrations of antimicrobials in PBS at 37 °C for 30 min, and then directly incubated with 10 µM of IQ-Cm or 5 µg/mL of PI in PBS at room temperature. The corresponding fluorescence spectra were recorded on a spectrofluorometer (Perkin Elmer LS 55). The antimicrobial activity was calculated based on the equation $[(I - I_0)/(I_{\max} - I_0)] \times 100$, where I is the fluorescence intensity of *E. coli* suspensions with treatment of antimicrobials, I_0 is the fluorescence intensity of *E. coli* suspensions without treatment (IQ-Cm at 600 nm or PI at 615 nm) and I_{\max} is the maximum achievable fluorescence intensity of the *E. coli* suspensions with the treatment of different concentrations of antimicrobials. The traditional agar plate culture was conducted to calculate the corresponding antimicrobial activity according to reference [31]: After *E. coli* suspensions treated with different concentrations of antimicrobials in PBS at 37 °C for 30 min, the solutions were diluted by 10^4 times with PBS. Next, 100 µL of diluted *E. coli* suspension was spread on LB agar plate and cultured at 37 °C for 14–16 h. The experiments were conducted in triplicate. The antimicrobial activity was calculated by the equation $[(A - B)/A] \times 100\%$, where A is the mean *E. coli* colony number grown on LB agar plate in the control group without the antimicrobial treatment, and B is the mean *E. coli* colony number grown on LB agar plate with the antimicrobial treatment. To determine MBC values, the curve of the antibacterial activity of the antimicrobials against their logarithm concentration was fitted by the function model DoseResp in the Growth/Sigmoidal category by software OriginPro 9.0.

Bacteria staining and imaging: To monitor the membranolytic action of antimicrobials on *E. coli*, the *E. coli* suspensions were treated with different concentrations of CTAB in PBS and then stained with IQ-Cm (10 µM) or PI (5 µg/mL) in PBS, as described in the evaluation of the antimicrobial activity experiments. Then, these *E. coli* suspensions were concentrated by centrifuging at 7100 rpm for 2 min. A total of 2 µL of the 10-times concentrated suspension was placed on the glass slide, covered with a coverslip, and then imaged on a fluorescence microscope with a ×100 oil lens (Upright Biological Microscope Ni-U). Imaging conditions for IQ-Cm: excitation filter = 460–490 nm, dichroic mirror = 505 nm,

emission filter = 515 nm long pass; for PI: excitation filter = 510–550 nm, dichroic mirror = 570 nm, emission filter = 590 nm long pass. To monitor the membranolytic action of CTAB on *E. coli* under a different incubation time, similar procedures were followed with the fixed CTAB concentration of 20 μM and varied incubation time with *E. coli*.

Scanning electron microscopy (SEM): The morphological change of *E. coli* with the antimicrobial treatment was observed by SEM (Carl Zeiss GeminiSEM 300, Jena, Germany), referring to the literature [32]. *E. coli* suspensions ($\sim 2 \times 10^7$ CFU/mL) were treated with different concentrations of CTAB in PBS at 37 °C for 30 min, and then 0.5% glutaraldehyde PBS solution was added to fix the *E. coli* for about 30 min. After centrifuging to remove the supernatant, 50 μL of sterile water was added to disperse the remaining *E. coli*. A total of 5 μL of *E. coli* suspension was transferred to a silicon slice, dried naturally, and then fixed with 0.1% glutaraldehyde overnight. Next, the *E. coli* sample was washed with sterile water and then gradient-dehydrated with an ethanol solution with volume fractions of 60%, 70%, 90% and 100%, respectively. After vacuum drying, the as-prepared samples were sprayed with platinum prior to observation.

3. Results and Discussion

Escherichia coli (*E. coli*), one of the most representative Gram-negative species, was chosen for demonstration. After being incubated with IQ-Cm, *E. coli* in three physiological states were observed with three cases in the fluorescence field of the fluorescence microscope. As shown in Figure 1a, *E. coli* exhibit orange, green and weak/negligible emissions after being stained with IQ-Cm as compared to the bright field image. Propidium iodide (PI) is a probe that only enters the dead bacteria with impaired CM and emits a red fluorescence [33]. Co-staining with PI, the red emission of PI was found only in the orange-colored *E. coli*, suggesting the orange-colored *E. coli* are dead with destroyed CM. Vice versa, *E. coli* with green or negligible emissions are alive. This observation is consistent with our previous work [19]. IQ-Cm cannot stain healthy *E. coli* due to the barrier function of OM and has a dim emission [34]. Once their OM becomes defective, IQ-Cm is allowed to be inserted into the low-polarity lipid membrane of *E. coli* and emits a green fluorescence [35]. Additionally, when their CM is further destroyed, IQ-Cm is located in the cytoplasm with a large polar surrounding and emits a red-shift orange fluorescence based on the TICT effect [36]. These distinctive fluorescence responses of IQ-Cm to the three states of *E. coli* favor the monitoring of the antimicrobial-induced bacterial membrane damage and make it suitable for the bacterial viability assay. To verify it, IQ-Cm was incubated with live and dead *E. coli* and their fluorescence spectra were recorded (Figure 1b). A weak emission was observed for live *E. coli* and a boosted orange emission with a maximum at about 600 nm was observed for dead *E. coli* killed with 75% alcohol, which was also verified with the in situ fluorescence spectrum under a confocal microscope (Figure S1). The fluorescence intensity of IQ-Cm shows a linear relationship with the amount of dead *E. coli* ($R^2 = 0.97$) (Figure 1c). Additionally, IQ-Cm shows negligible toxicity to *E. coli*, where over 97% of bacterial viability is retained after being incubated with IQ-Cm at a concentration of up to 10 μM and still 90% at 20 μM (Figure 1d). These properties of IQ-Cm are desired as a probe for assessing the activity of membrane-active antimicrobials and visualizing their interaction with OM and CM of Gram-negative bacteria, which will be discussed in the following.

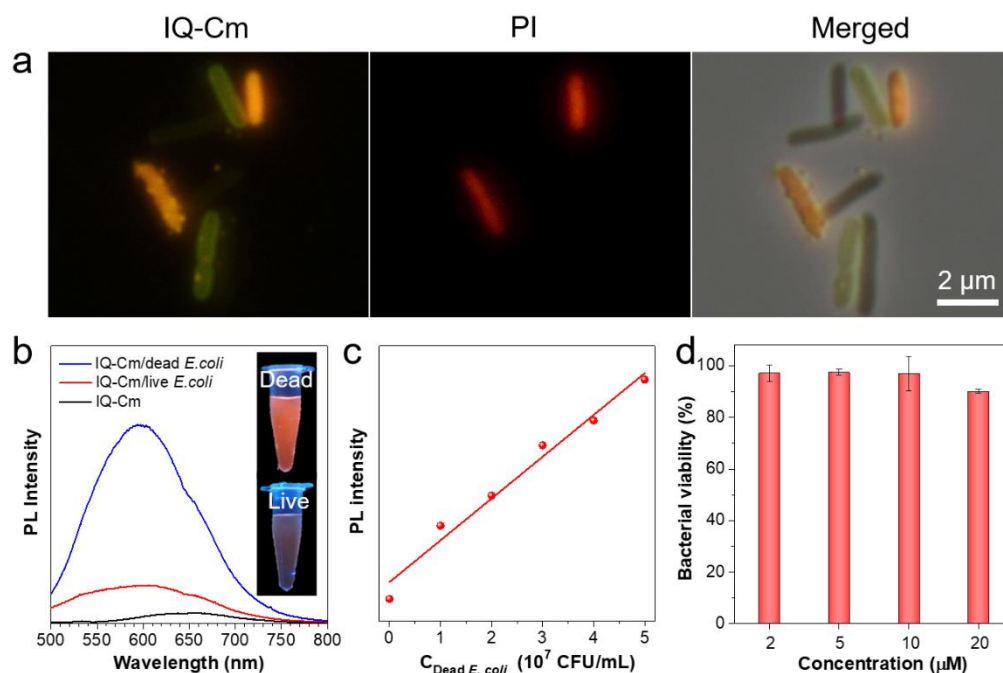


Figure 1. (a) Fluorescence images of *E. coli* incubated with IQ-Cm (10 μM) and PI (5 μg/mL) for 10 min. For IQ-Cm, excitation filter = 460–490 nm, dichroic mirror = 505 nm, emission filter = 515 nm long pass; for PI, excitation filter = 510–550 nm, dichroic mirror = 570 nm, emission filter = 590 nm long pass. (b) Fluorescence spectra of IQ-Cm (10 μM) in PBS solution before and after the addition of live *E. coli* or dead *E. coli*. (*E. coli* were killed by the treatment of 75% ethanol in water). Excitation wavelength: 450 nm. (c) Plot of emission intensity of IQ-Cm at 600 nm in the presence of various concentrations of dead *E. coli* in PBS solution. (d) The viability of *E. coli* stained with different concentrations of IQ-Cm.

Further IQ-Cm were used to assess the activity of membrane-active antimicrobials. Three commercial amphiphilic antimicrobials, i.e., hexadecyl trimethyl ammonium bromide (CTAB), dodecyl dimethyl benzyl ammonium bromide (DDBAB) and dodecyl trimethyl ammonium bromide (DTAB), which have different quaternary ammonium head groups and alkyl chain lengths and thus exert different antimicrobial potency, were chosen as representatives (Scheme 1c). Membrane-active antimicrobials kill Gram-negative bacteria by damaging OM and CM [4,37]. This opens the access of IQ-Cm to the bacterial cytoplasm, giving rise to the orange emission. *E. coli* were treated with different concentrations of antimicrobials for 30 min, followed by the staining of IQ-Cm. As shown in Figure 2a–c, the emission intensity of IQ-Cm gradually increases with the increasing concentration of antimicrobials. The emission intensity of IQ-Cm reaches its maximum at a concentration of up to 30 μM for CTAB, 30 μM for DDBAB and 200 μM for DTAB, respectively, suggesting all *E. coli* are almost killed. Meanwhile, it was found that antimicrobials alone do not cause an obvious change in emission of IQ-Cm (Figure S2). Given the linear relationship of fluorescence intensity of IQ-Cm with the dead *E. coli* concentration (Figure 1c), the killing efficiency of antimicrobials at various concentrations can be calculated by the equation $[(I - I_0)/(I_{\max} - I_0)] \times 100\%$, where I is the fluorescence intensity of *E. coli* treated with antimicrobials, I_{\max} is the achievable maximum intensity of *E. coli* treated with antimicrobials and I_0 is the intensity of the control *E. coli* group without antimicrobials. Minimal bactericidal concentration (MBC), an important parameter describing the antimicrobial effectiveness, can be easily determined from the plots in Figure 2d–f for the three antimicrobials. Their MBC₉₀ (the concentration of the antimicrobials to kill 90% of the bacteria) were evaluated as 14.3, 29.7 and 91.4 μM for CTAB, DDBAB and DTAB against *E. coli*, respectively. The traditional agar plate culture, a standard method, was performed, which shows very similar MBC₉₀ results of 14.8, 27.1 and 94.9 μM for CTAB, DDBAB and DTAB,

respectively (Figure 2g–i). In contrast, PI, the standard dead cell probe, had a MBC_{90} value of $25.8 \mu\text{M}$ for CTAB against *E. coli* (Figure S3), which is greatly deviated from the traditional agar plate culture method ($14.8 \mu\text{M}$). These results fully confirm the reliability of IQ-Cm for the activity assessment of membrane-active antimicrobials. Moreover, this fluorescence method is simple and timesaving with only 1~2 h needed, while the agar plate culture needs skilled plating and 24 h to show results.

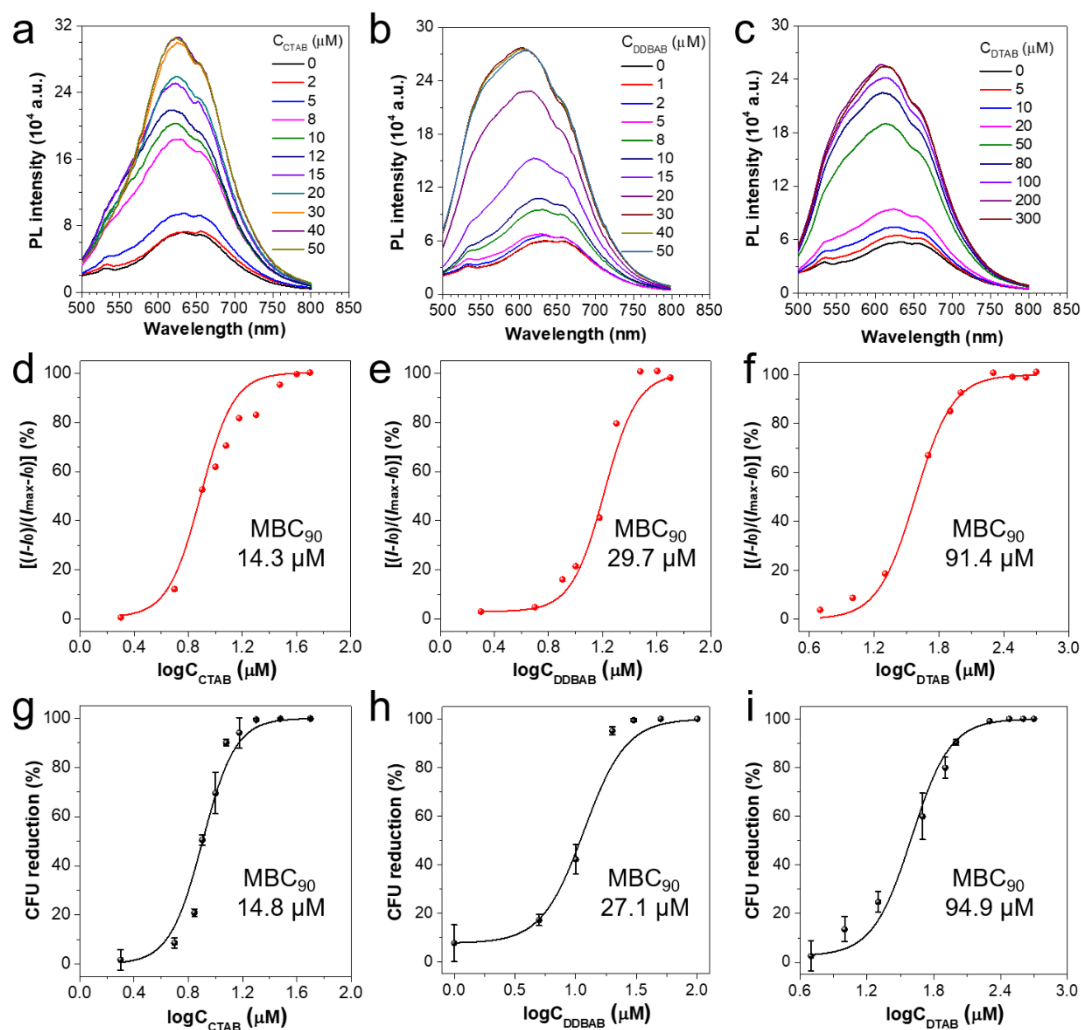


Figure 2. Evaluation of the activity of three antimicrobials. (a–c) Fluorescence spectra of *E. coli* suspension treated with different concentrations of antimicrobials and then stained with IQ-Cm ($10 \mu\text{M}$): (a) CTAB, (b) DDBAB and (c) DTAB. (d–f) Plots of $[(I - I_0)/(I_{max} - I_0)]$ versus antimicrobial concentration, where I and I_{max} correspond to the emission intensity and the achievable maximum intensity at 600 nm of the *E. coli* suspensions in the plots of a–c, respectively, and I_0 is the emission intensity of the *E. coli* suspension without the antimicrobial treatment; (d) CTAB, (e) DDBAB and (f) DTAB. (g–i) The plots of antibacterial activity of the three antimicrobials towards *E. coli* evaluated with the traditional agar plate culture method: (g) CTAB, (h) DDBAB and (i) DTAB.

To monitor the membranolytic action of antimicrobials on Gram-negative bacterial OM and CM, the fluorescence images of *E. coli* treated with different concentrations of CTAB and then stained with IQ-Cm were taken under a fluorescence microscope. As shown in Figure 3a, the emission color and location sites of IQ-Cm in bacteria depend on the CTAB concentration. In the control group without CTAB, *E. coli* show a negligible emission because of the barrier of the intact OM. After the addition of CTAB, the staining rate of *E. coli* with green or orange emission increases with increasing the CTAB concentration,

which is 50% for 6 μM , 80% for 8 μM , 99% for 12 μM and 100% for >15 μM of CTAB (Figure 3a,b). This indicates that CTAB compromises the membrane integrity of *E. coli*, allowing IQ-Cm to be inserted into the bacterial membrane of OM-defective *E. coli* or further accumulate in the cytoplasm of CM-disruptive *E. coli*. As a result, *E. coli* show green or orange fluorescence. The proportion of two colors was also found to rely on the CTAB concentration (Figure 3a), which reflects the extent of bacterial OM and CM disrupted by CTAB. At the low concentration of less than 8 μM , IQ-Cm-stained *E. coli* mainly show green emission (Figure 3a) and the ratio of green emission (530 nm) and orange emission (600 nm) is below 1.0 (Figure 3c). A total of 6 μM of CTAB, as an example, killed less than 20% of *E. coli*, which is much lower than the 50% staining rate of *E. coli* by IQ-Cm (Figure 3b). These results reveal that, at low concentrations, CTAB primarily compromises the physical integrity of Gram-negative bacteria OM, presumably due to the electrostatic interactions of quaternary ammonium of CTAB with the LPS on the OM of *E. coli* [4,15].

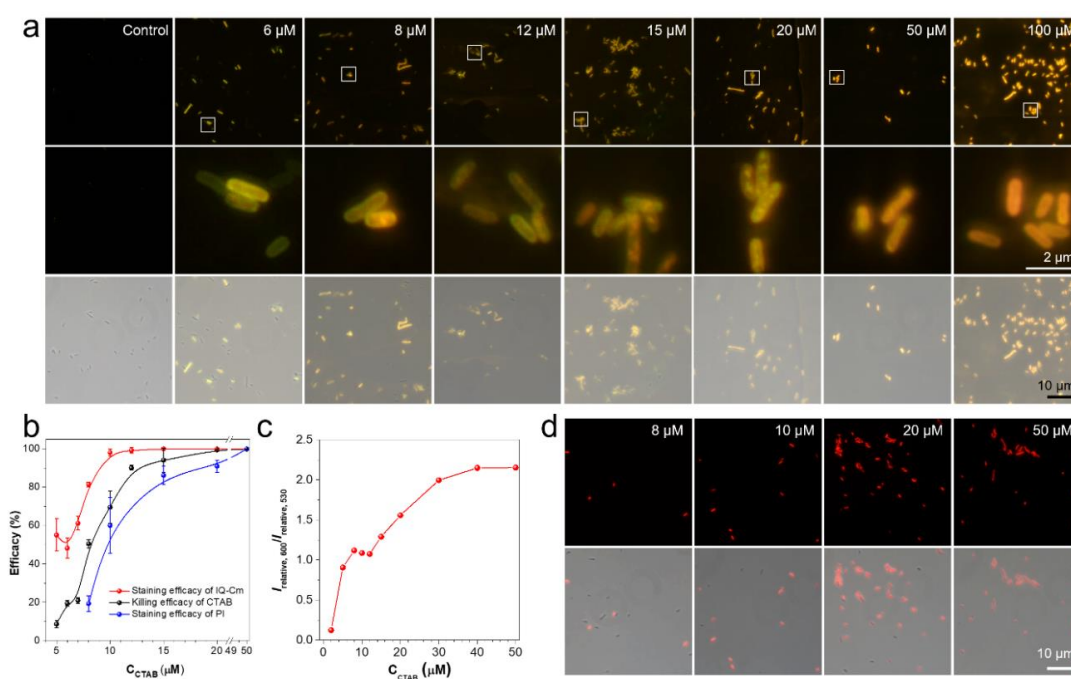


Figure 3. Visualization of the activity of antimicrobials under different concentrations. (a) Fluorescence images and merged images of *E. coli* treated by different concentrations of CTAB for 30 min and then stained by 10 μM of IQ-Cm for 10 min (The second row of images are the enlarged images of chosen white square areas in the first row of images). Excitation filter = 460–490 nm, dichroic mirror = 505 nm, emission filter = 515 nm long pass. (b) The plots of the staining efficacy of IQ-Cm and PI for *E. coli* and the antibacterial activity of CTAB against *E. coli* versus the concentration of CTAB. (c) The plots of the ratio of emission intensities at 600 nm and at 530 nm of IQ-Cm in the presence of *E. coli* treated with different concentrations of CTAB (The data obtained from Figure 2a). (d) Fluorescence and merged images of *E. coli* treated with CTAB for 30 min and then stained with 5 $\mu\text{g}/\text{mL}$ of PI for 10 min.

As the CTAB concentration increased to 8–15 μM , clearly most of IQ-Cm-stained *E. coli* exhibit green emission from their cell membrane and orange emission from their cytoplasm (Figure 3a). This means that a higher concentration of CTAB increases the permeability of both OM and CM of *E. coli*. Consequently, IQ-Cm could insert into the cell membrane and enter the cytoplasm of *E. coli* to have green and orange emissions. However, at this concentration range, the killing activity of CTAB against *E. coli* is still lower than the staining rate of *E. coli* by IQ-Cm (Figure 3b). This can be explained by the existence of the case where CTAB slightly affects the CM of *E. coli* without leading to a lethal event, as confirmed by the existence of green *E. coli* with faint orange fluorescence (Figure 3a).

Upon further increasing the CTAB concentration to more than 15 μM , the killing activity of CTAB against *E. coli* almost coincides with the staining rate of *E. coli* by IQ-Cm, close to the unity (Figure 3b). Almost all *E. coli* show a prominent orange emission (Figure 3a) with the ratio of intensities at 600 nm and 530 nm larger than 1 (Figure 3c). The SEM images show that the *E. coli* obviously collapse after being treated with this concentration range of CTAB, compared with the intact structures in control groups without CTAB treatment (Figure S4). Furthermore, after being treated with 100 μM of CTAB, the all-stained *E. coli* show an orange emission. This means that at high concentrations of $>15 \mu\text{M}$, CTAB significantly disrupts the OM and CM of *E. coli*.

In contrast, the conventional PI probe has a much lower staining rate of *E. coli* than that by IQ-Cm (Figure 3b,d), because PI cannot respond to OM changes and only has a red emission when allowed to penetrate into the microbe to bind with cytoplasm DNA [33]. In addition, the staining rate of *E. coli* by PI is also lower than the killing activity of CTAB against *E. coli* at the concentration below 20 μM (Figure 3b), leading to the above-mentioned higher MBC_{90} value assessed by the PI probe.

These fluorescence imaging results fully confirm that IQ-Cm as an indicator enables us to visualize the interactions of CTAB with the OM and CM of Gram-negative bacteria. It was revealed that CTAB interacts with the OM and CM of Gram-negative bacteria in a dose-dependent manner. At a low concentration, CTAB primarily compromises the OM of *E. coli*. At a medium concentration, additional CTAB further interact with the CM of *E. coli* and disrupts the CM of some *E. coli*, making CTAB exhibit mediate antimicrobial activity. At high concentrations, sufficient CTAB significantly disrupts both the OM and CM, thereby showing high killing activity against *E. coli*.

Furthermore, IQ-Cm was used to monitor the time course of membrane disruption of Gram-negative bacteria induced by membrane-active antimicrobials. We chose a CTAB concentration of 20 μM with the killing activity of 99.5% as an example. As shown in Figure 4a, after incubated with CTAB for less than 20 min and then stained by IQ-Cm, some *E. coli* exhibit green or green with faint orange, and the staining rate of *E. coli* by IQ-Cm is obviously larger than that by PI (Figure 4b and Figure S5). This means CTAB initially disrupts the OM integrity of *E. coli* and short incubation time is not sufficient for CTAB to fully destroy the CM of *E. coli*. Upon extending the incubation time to 25 and 30 min, the cytoplasm of *E. coli* was almost all found to emit predominant orange fluorescence (Figure 4a). The staining efficiency of PI for *E. coli* is gradually closer to that of IQ-Cm (Figure 4b). These results suggest that 25 or 30 min of incubation time is required for 20 μM of CTAB to compromise the OM and CM of *E. coli* and thus sufficiently exert the antimicrobial activity. Above all, IQ-Cm was demonstrated to be highly suitable for visualizing the interaction of membrane-active antimicrobials with the OM and CM of Gram-negative bacteria.

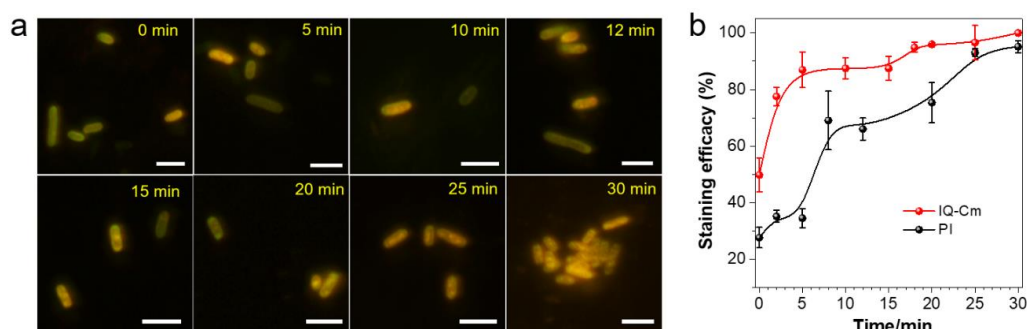


Figure 4. Visualization of the antimicrobial effect of antimicrobials with different incubation times. (a) Fluorescence images of *E. coli* treated with 20 μM of CTAB for different times and then stained with IQ-Cm (10 μM) for 10 min. Scale bar: 2 μm . (b) The staining efficacy of IQ-Cm and PI for *E. coli* versus the incubation time of *E. coli* with CTAB.

4. Conclusions

In summary, a microenvironment-sensitive bicolor AIEgen was applied to achieve the visual monitoring of the interaction between membrane-active antimicrobials and Gram-negative bacterial membrane. The disruption of OM and CM by antimicrobials was clearly indicated based on two discernable green and orange emissions of IQ-Cm responding to OM-defective and CM-disruptive Gram-negative bacteria, respectively. Moreover, IQ-Cm was used to study the dose-dependence and incubation time-dependence of antimicrobials. The low concentration of antimicrobials (or short incubation time) primarily compromises the OM of bacteria, and the high concentration of antimicrobials (or extending incubation time) significantly disrupts the OM and CM. Additionally, based on the great emission difference of IQ-Cm to live and dead *E. coli*, the activity of antimicrobials can be easily assessed with acceptable accuracy within 1~2 h, faster than the agar plate culture method (24 h). Our studies may advance the understanding for the interaction of membrane-active antimicrobials with the OM and CM of Gram-negative bacteria and facilitate the design and development of antimicrobials.

Supplementary Materials: The following supporting information can be downloaded at: <https://www.mdpi.com/article/10.3390/chemosensors10070284/s1>. Figure S1: In situ fluorescence spectrum of dead *E. coli* stained with IQ-Cm; Figure S2: The effect of antimicrobials on the emission spectra of IQ-Cm; Figure S3: Evaluation of antimicrobial activity of CTAB by PI probe. Figure S4: SEM characterization of *E. coli* morphology after CTAB treatment; Figure S5: Visualization of activity of CTAB against *E. coli* with different incubation times by fluorescence imaging using PI.

Author Contributions: C.Z.: Conceptualization, methodology, investigation, formal analysis, data curation, visualization, writing—original draft, funding acquisition; Z.D.: Investigation; Q.G.: Investigation; M.J.: Conceptualization, resources, supervision, writing—review and editing. All authors have read and agreed to the published version of the manuscript.

Funding: We appreciate the financial support from the National Natural Science Foundation of China (22002137), the Natural Science Foundation of Jiangsu Province (BK20200920), the Double PhD Program of Jiangsu Province (JSSCBS20211067), “Green Yang and Gold Golden Phoenix Plan” of Yangzhou City (YZLYJF2020PHD118) and Yangzhou University Interdisciplinary Research Foundation for Chemistry Discipline of Targeted Support (yzuxk202012).

Institutional Review Board Statement: Not applicable.

Informed Consent Statement: Not applicable.

Data Availability Statement: Not applicable.

Conflicts of Interest: The authors declare no conflict of interest.

References

1. Casadevall, A.; Pirofski, L.-A. Microbiology: Ditch the term pathogen. *Nature* **2014**, *516*, 165. [[CrossRef](#)] [[PubMed](#)]
2. Xu, Z.; Qiu, Z.; Liu, Q.; Huang, Y.; Li, D.; Shen, X.; Fan, K.; Xi, J.; Gu, Y.; Tang, Y.; et al. Converting organosulfur compounds to inorganic polysulfides against resistant bacterial infections. *Nat. Commun.* **2018**, *9*, 3713. [[CrossRef](#)] [[PubMed](#)]
3. Rojas, E.R.; Billings, G.; Odermatt, P.D.; Auer, G.K.; Zhu, L.; Miguel, A.; Chang, F.; Weibel, D.B.; Theriot, J.A.; Huang, K.C. The outer membrane is an essential load-bearing element in Gram-negative bacteria. *Nature* **2018**, *559*, 617–621. [[CrossRef](#)] [[PubMed](#)]
4. Lam, S.J.; O'Brien-Simpson, N.M.; Pantarat, N.; Sulistio, A.; Wong, E.H.H.; Chen, Y.-Y.; Lenzo, J.C.; Holden, J.A.; Blencowe, A.; Reynolds, E.C.; et al. Combating multidrug-resistant Gram-negative bacteria with structurally nanoengineered antimicrobial peptide polymers. *Nat. Microbiol.* **2016**, *1*, 16162. [[CrossRef](#)]
5. Jones, S. Permeability rules for antibiotic design. *Nat. Biotechnol.* **2017**, *35*, 639. [[CrossRef](#)]
6. Xu, Z.-Q.; Flavin, M.T.; Flavin, J. Combating multidrug-resistant Gram-negative bacterial infections. *Exp. Opin. Investig. Drugs* **2014**, *23*, 163–182. [[CrossRef](#)]
7. Lee, J.H.; Jeong, S.H.; Cha, S.-S.; Lee, S.H. A lack of drugs for antibiotic-resistant Gram-negative bacteria. *Nat. Rev. Drug Discov.* **2007**, *6*, 938. [[CrossRef](#)]
8. Zhou, C.; Wang, Y. Structure-activity relationship of cationic surfactants as antimicrobial agents. *Curr. Opin. Colloid Interface Sci.* **2020**, *45*, 28–43. [[CrossRef](#)]
9. Qi, R.; Zhang, P.; Liu, J.; Zhou, L.; Zhou, C.; Zhang, N.; Han, Y.; Wang, S.; Wang, Y. Peptide amphiphiles with distinct supramolecular nanostructures for controlled antibacterial activities. *ACS Appl. Bio Mater.* **2018**, *1*, 21–26. [[CrossRef](#)]

10. Ergene, C.; Yasuhara, K.; Palermo, E.F. Biomimetic antimicrobial polymers: Recent advances in molecular design. *Polym. Chem.* **2018**, *9*, 2407–2427. [[CrossRef](#)]
11. Liu, S.Q.; Venkataraman, S.; Ong, Z.Y.; Chan, J.M.; Yang, C.; Hedrick, J.L.; Yang, Y.Y. Overcoming multidrug resistance in microbials using nanostructures self-assembled from cationic bent-core oligomers. *Small* **2014**, *10*, 4130–4135. [[CrossRef](#)] [[PubMed](#)]
12. Pinazo, A.; Manresa, M.A.; Marques, A.M.; Bustelo, M.; Espuny, M.J.; Perez, L. Amino acid-based surfactants: New antimicrobial agents. *Adv. Colloid Interface Sci.* **2016**, *228*, 17–39. [[CrossRef](#)]
13. Randall, C.P.; Mariner, K.R.; Chopra, I.; O'Neill, A.J. The target of daptomycin is absent from *Escherichia coli* and other gram-negative pathogens. *Antimicrob. Agents Chemother.* **2013**, *57*, 637–639. [[CrossRef](#)] [[PubMed](#)]
14. Pitsalidis, C.; Pappa, A.M.; Porel, M.; Artim, C.M.; Faria, G.C.; Duong, D.D.; Alabi, C.A.; Daniel, S.; Salleo, A.; Owens, R.M. Biomimetic electronic devices for measuring bacterial membrane disruption. *Adv. Mater.* **2018**, *30*, 1803130. [[CrossRef](#)] [[PubMed](#)]
15. Yasuda, K.; Ohmizo, C.; Katsu, T. Potassium and tetraphenylphosphonium ion-selective electrodes for monitoring changes in the permeability of bacterial outer and cytoplasmic membranes. *J. Microbiol. Meth.* **2003**, *54*, 111–115. [[CrossRef](#)]
16. Bisoyi, H.K.; Li, Q. Liquid crystals: Versatile self-organized smart soft materials. *Chem. Rev.* **2022**, *122*, 4887–4926. [[CrossRef](#)]
17. Rodriguez-Rivera, F.P.; Zhou, X.; Theriot, J.A.; Bertozzi, C.R. Visualization of mycobacterial membrane dynamics in live cells. *J. Am. Chem. Soc.* **2017**, *139*, 3488–3495. [[CrossRef](#)]
18. Cao-Hoang, L.; Marechal, P.A.; Lê-Thanh, M.; Gervais, P.; Waché, Y. Fluorescent probes to evaluate the physiological state and activity of microbial biocatalysts: A guide for prokaryotic and eukaryotic investigation. *Biotechnol. J.* **2008**, *3*, 890–903. [[CrossRef](#)]
19. Zhou, C.; Jiang, M.; Du, J.; Bai, H.; Shan, G.; Kwok, R.T.K.; Chau, J.H.C.; Zhang, J.; Lam, J.W.Y.; Huang, P.; et al. One stone, three birds: One AIEgen with three colors for fast differentiation of three pathogens. *Chem. Sci.* **2020**, *11*, 4730–4740. [[CrossRef](#)]
20. Chen, X.-M.; Feng, W.-J.; Bisoyi, H.K.; Zhang, S.; Chen, X.; Yang, H.; Li, Q. Light-activated photodeformable supramolecular dissipative self-assemblies. *Nat. Commun.* **2022**, *13*, 3216. [[CrossRef](#)]
21. Hoque, J.; Akkapeddi, P.; Yarlagadda, V.; Uppu, D.S.; Kumar, P.; Haldar, J. Cleavable cationic antibacterial amphiphiles: Synthesis, mechanism of action, and cytotoxicities. *Langmuir* **2012**, *28*, 12225–12234. [[CrossRef](#)] [[PubMed](#)]
22. Mei, J.; Leung, N.L.; Kwok, R.T.; Lam, J.W.; Tang, B.Z. Aggregation-induced emission: Together we shine, united we soar! *Chem. Rev.* **2015**, *115*, 11718–11940. [[CrossRef](#)]
23. Zhou, C.; Xu, W.; Zhang, P.; Jiang, M.; Chen, Y.; Kwok, R.T.K.; Lee, M.M.S.; Shan, G.; Qi, R.; Zhou, X.; et al. Engineering sensor arrays using aggregation-induced emission luminogens for pathogen identification. *Adv. Funct. Mater.* **2019**, *29*, 1805986. [[CrossRef](#)]
24. Jiang, M.; Gu, X.; Lam, J.W.; Zhang, Y.; Kwok, R.T.; Wong, K.S.; Tang, B.Z. Two-photon AIE bio-probe with large stokes shift for specific imaging of lipid droplets. *Chem. Sci.* **2017**, *8*, 5440–5446. [[CrossRef](#)] [[PubMed](#)]
25. Wang, N.; Yao, H.; Tao, Q.; Sun, J.; Ma, H.; Wang, Y.; Zhou, C.; Fan, H.; Shao, H.; Qin, A.; et al. TPE based aggregation induced emission fluorescent sensors for viscosity of liquid and mechanical properties of hydrogel. *Chin. Chem. Lett.* **2022**, *33*, 252–256. [[CrossRef](#)]
26. Kang, M.; Zhang, Z.; Song, N.; Li, M.; Sun, P.; Chen, X.; Wang, D.; Tang, B.Z. Aggregation-enhanced theranostics: AIE sparkles in biomedical field. *Aggregate* **2020**, *1*, 80–106. [[CrossRef](#)]
27. Nie, H.; Wei, Z.; Ni, X.-L.; Liu, Y. Assembly and applications of macrocyclic-confinement-derived supramolecular organic luminescent emissions from cucurbiturils. *Chem. Rev.* **2022**, *122*, 9032–9077. [[CrossRef](#)]
28. Yu, Z.; Duan, Y.; Cheng, L.; Han, Z.; Zheng, Z.; Zhou, H.; Wu, J.; Tian, Y. Aggregation induced emission in the rotatable molecules: The essential role of molecular interaction. *J. Mater. Chem.* **2012**, *22*, 16927–16932. [[CrossRef](#)]
29. Liese, D.; Haberhauer, G. Rotations in excited ICT states—fluorescence and its microenvironmental sensitivity. *Isr. J. Chem.* **2018**, *58*, 813–826. [[CrossRef](#)]
30. Cheng, Y.; Wang, J.; Qiu, Z.; Zheng, X.; Leung, N.L.; Lam, J.W.; Tang, B.Z. Multiscale humidity visualization by environmentally sensitive fluorescent molecular rotors. *Adv. Mater.* **2017**, *29*, 1703900. [[CrossRef](#)]
31. Xing, C.; Xu, Q.; Tang, H.; Liu, L.; Wang, S. Conjugated polymer/porphyrin complexes for efficient energy transfer and improving light-activated antibacterial activity. *J. Am. Chem. Soc.* **2009**, *131*, 13117–13124. [[CrossRef](#)]
32. Bai, H.; Yuan, H.; Nie, C.; Wang, B.; Lv, F.; Liu, L.; Wang, S. A supramolecular antibiotic switch for antibacterial regulation. *Angew. Chem. Int. Ed.* **2015**, *54*, 13208–13213. [[CrossRef](#)] [[PubMed](#)]
33. Sträuber, H.; Müller, S. Viability states of bacteria—specific mechanisms of selected probes. *Cytom. Part A* **2010**, *77*, 623–634. [[CrossRef](#)]
34. Wang, Y.; Corbitt, T.S.; Jett, S.D.; Tang, Y.; Schanze, K.S.; Chi, E.Y.; Whitten, D.G. Direct visualization of bactericidal action of cationic conjugated polyelectrolytes and oligomers. *Langmuir* **2012**, *28*, 65–70. [[CrossRef](#)] [[PubMed](#)]
35. Dowhan, W. Molecular basis for membrane phospholipid diversity: Why are there so many lipids? *Annu. Rev. Biochem.* **1997**, *66*, 199–232. [[CrossRef](#)] [[PubMed](#)]
36. Fushimi, K.; Verkman, A.S. Low viscosity in the aqueous domain of cell cytoplasm measured by picosecond polarization microfluorimetry. *J. Cell Biol.* **1991**, *112*, 719–725. [[CrossRef](#)]
37. Zhou, C.; Wang, F.; Chen, H.; Li, M.; Qiao, F.; Liu, Z.; Hou, Y.; Wu, C.; Fan, Y.; Liu, L.; et al. Selective antimicrobial activities and action mechanism of micelles self-assembled by cationic oligomeric surfactants. *ACS Appl. Mater. Interfaces* **2016**, *8*, 4242–4249. [[CrossRef](#)]